JOURNAL OF SOLID STATE CHEMISTRY **126,** 253–260 (1996)
ARTICLE NO. 0336

Stoichiometry, Defects, and Ordering in Lead Tantalum Oxides with Pyrochlore-Related Structures

N. Menguy, F. Thuriès, and C. Caranoni

Laboratorie Matériaux, Organisation et Propriétés, URA CNRS 1530, Universite d'Aix-Marseille III, case 151, Faculte des Sciences, Avenue Escadrille Normandie-Niemen, F-13397 Marseille Cedex 20, France

Received March 21, 1996; accepted May 31, 1996

The phase diagram in the $PbO–Ta_2O_5$ system has been reinvestigated in the $Pb_{1.5}Ta_2O_{6.5}$–$Pb_{2.44}Ta_2O_{7.44}$ composition range. The existence of the defect-pyrochlore cubic phase $Pb_{1.5}Ta_2O_{6.5}$ is confirmed but the apparent solid solution previously reported in the $Pb_{2.31}Ta_2O_{7.31}$–$Pb_{2.44}Ta_2O_{7.44}$ composition range is shown to be due to the coherent intergrowth of defined rhombohedral phases with slightly different compositions.

INTRODUCTION

It is well known that ordering of extended defects can generate a succession of crystallographically defined structures, closely spaced in composition and closely related in structure to each other and to the host structure (1, 2). For instance, such behavior has been experimentally observed in the case of lead niobates with a pyrochlore host structure. For $0 \leq x \leq 0.5$, the $Pb_{2+x}Nb_2O_{7+x}$ compounds exhibit structures which are derived from the ideal pyrochlore structure by periodic faulting on (111) planes. Depending on the ordering between stacking faults, four different rhombohedral structures have been obtained (3–7).

The coherent intergrowth of such phases can mimic the properties of a nonstoichiometric phase. From previous works, such behavior is suggested in the case of lead tantalates with a pyrochlore host structure. On the basis of X-ray diffraction results, a rhombohedral phase similar to one of those observed for lead niobates has been reported but the existence of a solid solution has also been proposed in the $Pb_{2.31}Ta_2O_{7.31}$–$Pb_{2.44}Ta_2O_{7.44}$ composition range (8). However, for the same composition range, four phases have been observed in the analogous $PbO–Nb_2O_5$ system (3–7). Because of these incertainities in the phase diagram, we reinvestigated the $PbO–Ta_2O_5$ system over the composition range in which pyrochlore-related phases are expected. Moreover, structural models related to the stacking fault have also been studied by high resolution electron microscopy.

SINGLE CRYSTAL SYNTHESIS

Single crystals of lead tantalates have been prepared using a conventional flux growth method. At first, a powder is prepared from a solid state reaction between constituent oxides mixed in the stoichiometric proportions 2 PbO/1 Ta_2O_5 and heated at 1273 K for 4 h.

It is worth noting that after the first stage of elaboration, the overall composition of the obtained powder leads to an atomic concentration ratio [Pb]/[Ta] = 1 consistent with the initial stoichiometric proportions. X-ray diffraction studies revealed that the powder consists actually of a mixing of two phases identified from JCPDS files as the defect cubic pyrochlore phase $Pb_{1.5}Ta_2O_{6.5}$ (a = 1.056 nm) and the rhombohedral phase $Pb_{22}Ta_{18}O_{67}$ (in hexagonal axes a = 0.747 nm, c = 4.813 nm) reported by Scott (8).

Then, single crystals were grown from a flux mixture of $PbF_2–PbO–B_2O_3$ submitted to the follwing thermal cycle: heating at 1423 K for 2 h, cooling to 1073 K at 5 K h^{-1}, then to 873 K at 10 K h^{-1}, followed by 50 K h^{-1} to room temperature. A single type of millimeter-sized single crystals with a yellow coloration was extracted from the matrix with hot dilute nitric acid. Their morphological shape is similar to a flat rhombohedron, with well developed basal planes, indicating a possible rhombohedral structure (Fig. 1a). A precise examination of the less developed faces of the crystals, e.g., the faces which are not perpendicular to the ternary axis, show a lamellar structure (Fig. 1b); the obtained single crystals have a layered structure with a stacking along the ternary axis. Nevertheless, it has to be noticed that there is a correlation between the observed shape of the crystals and the expected cubic symmetry as shown in Fig. 1c.

Compositional X-ray energy dispersive spectroscopy analyses were performed using a Philips 515 scanning electron microscope on single crystals yielding the chemical formula $Pb_{2.2}Ta_2O_{7.2}$ (called PTO hereafter).

0022-4596/96 $18.00

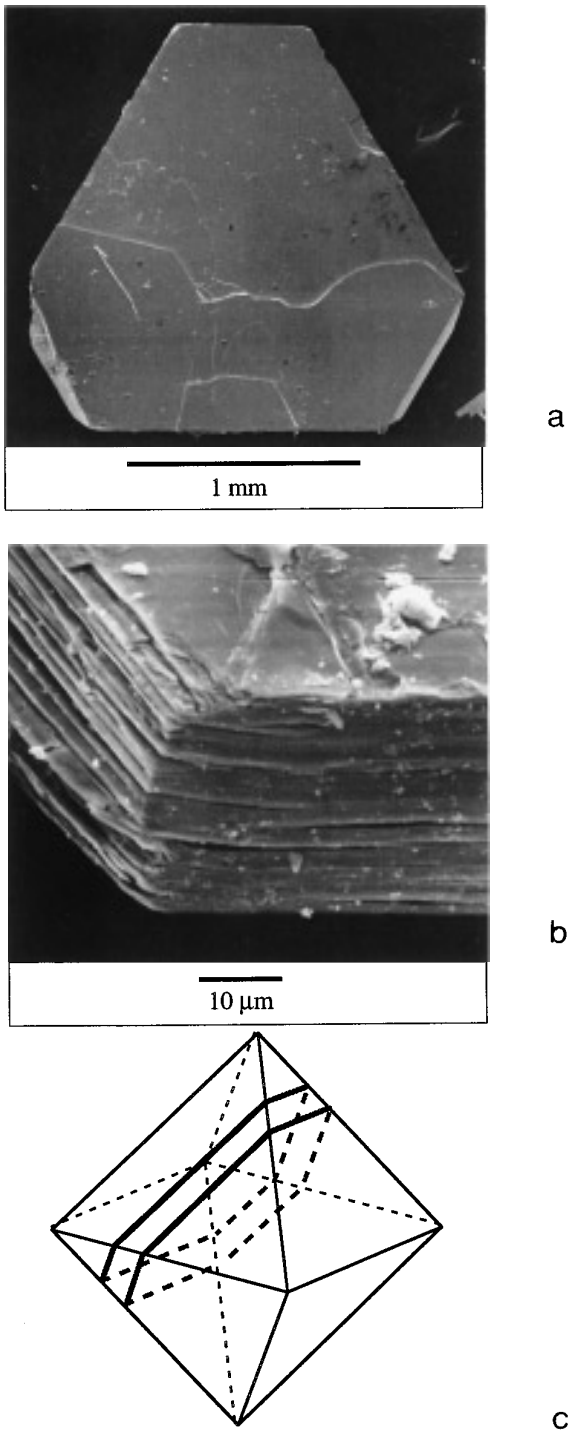

FIG. 1. SEM images (secondary electrons) of a PTO single crystal. (a) PTO single crystal observed along the ternary axis exhibiting a well developed face. (b) Lamellae stacked along the ternary axis. (c) Correlation between the shape of PTO single crystals and the cubic symmetry: the flat rhombohedron can be inscribed in an octahedron.

X-RAY DIFFRACTION ANALYSES

X-ray powder diffraction experiments have shown, in a first approach, that the structure of PTO crystals is similar to the rhombohedral phase $Pb_{22}Ta_{18}O_{67}$ observed in the powder from the first step elaboration. From these results it seems that after the second step of the elaboration procedure, described above, the defect cubic pyrochlore $Pb_{1.5}Ta_2O_{6.5}$ phase did not crystallize.

Our results are consistent with those reported by Scott (8). In his paper, Scott reports that his attempts to prepare the rhombohedral phase $Pb_2Ta_2O_7$ failed and, in each case, he obtained a mixture of the cubic defect-pyrochlore $Pb_{1.5}Ta_2O_{6.5}$ and a rhombohedral phase $Pb_{22}Ta_{18}O_{67}$ closely similar to our PTO crystals. As Scott did, we conclude that the widely reported rhombohedral phase $Pb_2Ta_2O_7$ (9–12), with the parameters $a = 0.747$ nm and $c = 1.924$ nm, does not exist.

Nevertheless, the chemical composition of the PTO single crystals we have prepared differs slightly from that reported by Scott. As suggested by Scott, this could be explained by the existence of a solid solution in the $Pb_{2.31}Ta_2O_{6.31}$–$Pb_{2.44}Ta_2O_{7.44}$ composition range but this difference could also result from the intergrowth of several phases with different stoichiometry in our PTO crystals. Insofar as X-ray diffraction studies give average structural information and may be unable to detect minority phases, transmission electron microscope experiments were carried out.

CONVENTIONAL TRANSMISSION ELECTRON MICROSCOPY

At first, electron diffraction experiments were performed using a Jeol 200 CX transmission electron microscope (TEM). One PTO crystal was crushed and deposited on a holey carbon film. From electron diffraction experiments, four different phases were observed: selecting area diffraction patterns (SADP) of the different phases observed along equivalent directions are shown in Fig. 2.

Figure 2a shows the SADP related to the most frequently observed phase, Fig. 2b corresponds to a ⟨110⟩ zone axis SADP related to the cubic pyrochlore structure, and Figs. 2c and 2d correspond to SADP related to the two other phases.

By comparison with the ⟨110⟩ zone axis SADP (Fig. 2b), it can be seen that the SADP shown in Fig. 2a is characterized by the existence of four superstructure reflections lying along the ternary axis and between intense reflections. Figures 2c and 2d show SADP exhibiting, respectively, six and eleven superstructure reflections between fundamental reflections. It can be pointed out that all the SADP have in common their intense reflections, suggesting that the four different structures have the same structural unit. As reported by Scott for the rhombohedral $Pb_{22}Ta_{18}O_{67}$ and by several authors for lead niobates (3–7), the intense reflections are characteristic of a distorted

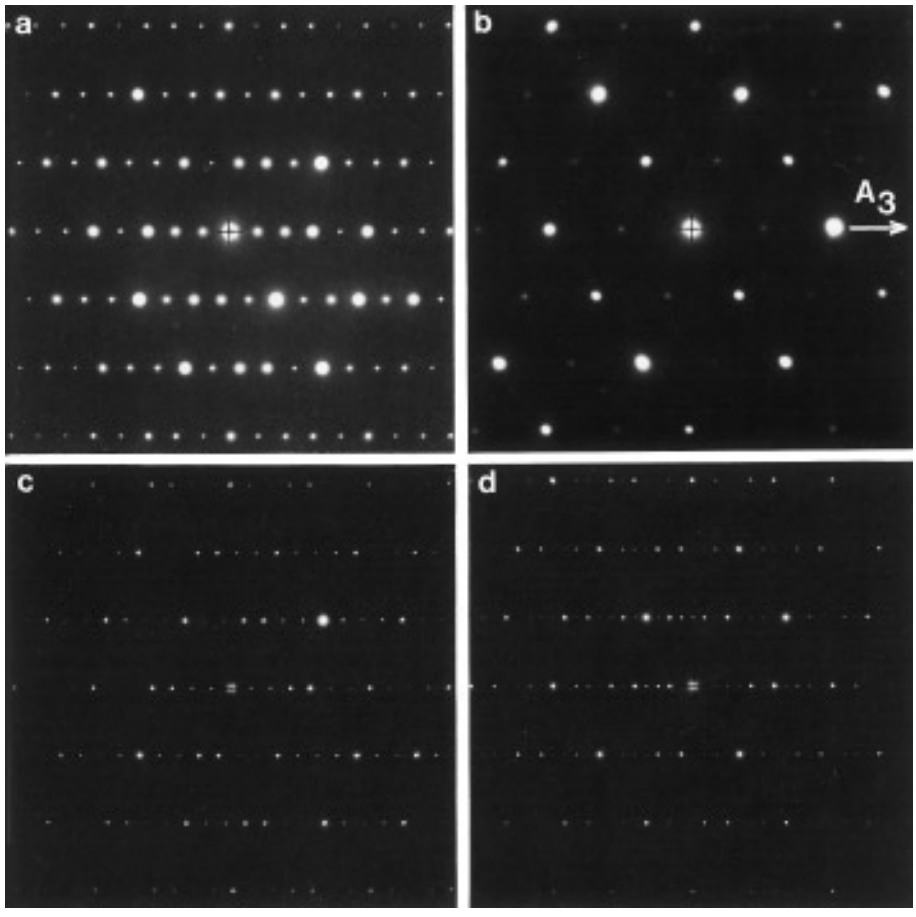

FIG. 2. Selected area diffraction patterns of the different phases in PTO crystals observed along equivalents directions. (a) SADP related to the most often observed phase. This electron diffraction pattern has to be compared with the SADP related to the cubic pyrochlore phase (b). In (a), four superstructure reflections lying along the ternary axis are visible between fundamental reflections. (c) and (d): SADP related to two other phases observed in PTO crystals, 6 and 11 superstructure reflections lying along the ternary axis are visible between fundamental reflections in, respectively, (c) and (d).

fluorite-type cell and superstructure reflections lying along the ternary axis (Figs. 2a, 2c, 2d) indicate the existence of periodic faulting on (111) planes.

A detailed study of the reciprocal space leads us to assume that these three phases are rhombohedral (13). The indexation of the different SADP shown in Figs. 2a, 2c, and 2d has been carried out using a hexagonal description (Fig. 3). It has to be noticed that these SADP exhibit fine Bragg spots indicating that the observed particles are constituted of homogeneous and well-defined phases.

On the basis of X-ray diffraction results related to lead niobates $Pb_{2+x}Nb_2O_{7+x}$ (3, 4, 6, 7) and lead tantalates (8), the a_{hex} parameter can be assumed to be equal for all the phases, and then the c_{hex} parameters have been deduced and all the parameters of the different cells are summarized in Table 1. The intergrowth of the different phases is shown in Fig. 4. This bright field image is characterized by the presence of an irregular array of fringes which strongly differ in contrast from the other fringes. These fringes whose contrast varies as a function of thickness correspond in fact to the stacking faults; for easier visualization, their positions are indicated in the lower part of the figure. Between each stacking fault, one can see a regular array of bright dots which corresponds to the normal octahedral layer stacking of the pyrochlore structure. To a defined and regular spacing between the planar defects corresponds a defined crystallographic structure; from the observation of this image, it can then be deduced that the intergrowth between the different structures is fully coherent.

An enlargement of a part of Fig. 4 is shown in Fig. 5. This part of the sample is characterized by the absence of stacking faults and corresponds consequently to the nonfaulted pyrochlore structure. Image analysis performed on this image has shown, on the basis of an a_{hex} parameter

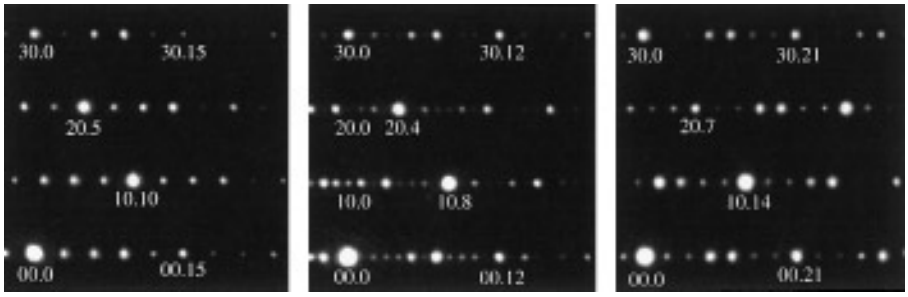

FIG. 3. (a), (b), and (c): Indexed SADP related to the different observed phases in PTO crystals. The indexation has been carried out using a hexagonal description of the different cells.

equal to 0.747 nm, that the c_{hex} parameter is equal to 1.825 nm. This indicates that the observed nonfaulted structure has the same c_{hex} parameter as the defect cubic pyrochlore structure $Pb_{1.5}Ta_2O_{6.5}$ with the $Fd\bar{3}m$ space group symmetry. As it has been shown that for an atomic concentration ratio $[Pb]/[B] > 0.75$ with B = Ta or Nb the cubic pyrochlore is not observed (8, 10, 11, 14–16), it can be supposed at least that the nonfaulted structure is a lead poor compound.

HIGH RESOLUTION ELECTRON MICROSCOPY (HREM) STUDY OF STACKING FAULTS

Figures 6a, 6b, and 6c show HREM images related to the faulted structures. All these images have been obtained along the same direction, e.g., the $[100]_{hex}$ zone axis. These HREM micrographs show layered structures constituted of blocks. These blocks are separated by stacking faults revealed by rows of bright dots perpendicular to the threefold axis as it will be confirmed later. For each phase, the c_{hex} parameter can be deduced from the repetition of the white dots along the threefold axis. Examination of Figs. 6a, 6b, and 6c leads to c_{hex} parameters, respectively, equal to 4.8, 6.7, and 3.8 nm, in agreement with electron diffraction results. Structures consist of the stacking of 3×5, 3×7, and $7 + 5$ layers, respectively. It has to be pointed out that the 3×5 and 3×7 structures have been previously observed in the case of lead niobates, whereas for lead tantalates only the 3×5 structure has been reported (3–8).

STRUCTURAL MODELS

Models for 3×5 and 3×7 structures have been proposed for lead niobates by Bernotat-Wulff *et al.* and Saine (6, 15). These models are derived from the stacking of the ideal cubic pyrochlore structure $A_2B_2O_7$. As shown in Fig. 7a, this structure can be described as the following sequence of octahedral layers stacked along the ⟨111⟩ directions: $\ldots \gamma\mathcal{A}\alpha\mathcal{B}\beta\mathcal{C}\gamma\mathcal{A}\ldots$, where $\mathcal{A}$, $\mathcal{B}$, and $\mathcal{C}$ are layers rich in A cations (3 A cations for 1 B cation) and α, β, and γ are layers rich in B cations (3 B cations for 1 A cation). The distinction between layers of the same type, e.g., symbolized with the same kind of letter (roman or Greek), is due to a translation perpendicular to the threefold direction. It is straightforward to see that the ideal

TABLE 1
Parameters of the Different Phases Observed in PTO Crystals

	Cubic phase	4 superstr. refl.	6 superstr. refl.	11 superstr. refl.
Cell parameters (nm)	$a_{cub} = 1.056$ $a_{hex} = 0.747$, $c_{hex} = 1.829$	$a_{hex} = 0.747$, $c_{hex} = 4.80$	$a_{hex} = 0.747$, $c_{hex} = 6.68$	$a_{hex} = 0.747$, $c_{hex} = 3.80$
Space group	$Fd\bar{3}m$	$R3m$ $R\bar{3}m$ $R32$	$R3m$ $R\bar{3}m$ $R32$	$P3m1$ $P321$
Number of layers	6	15	21	12
Layer thickness (nm)	0.305	0.320	0.318	0.317
Theoretical [Pb]/[Ta]		1.22	1.15	1.18

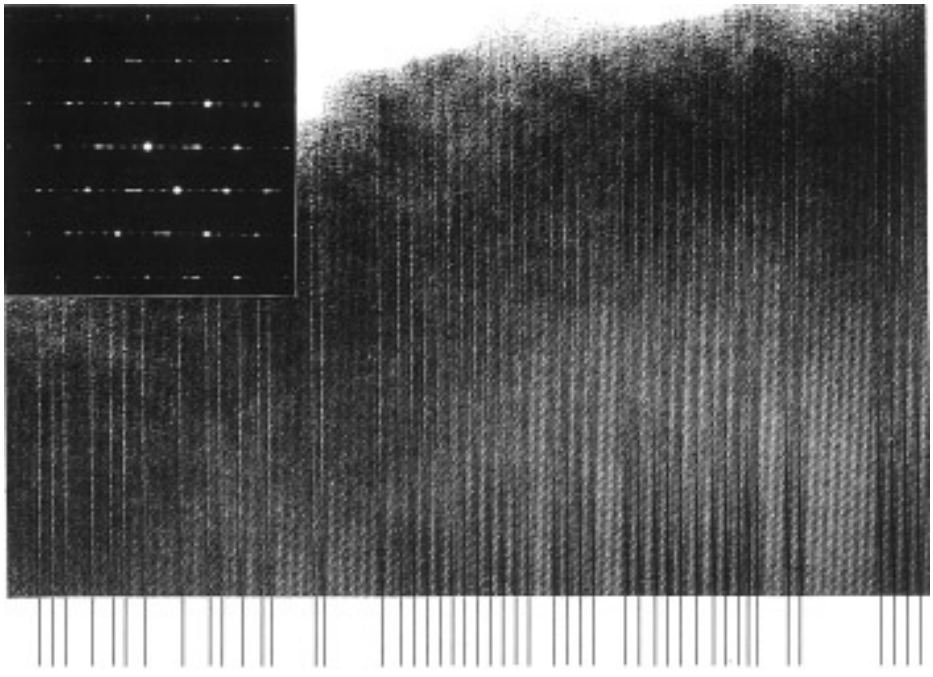

FIG. 4. Bright field image of a PTO particle and corresponding SADP showing the coherent intergrowth of the different phases. Positions of the stacking faults are indicated by thin lines. These stacking faults are perpendicular to the plan view and to the ternary axis. To the irregular array of these stacking faults corresponds a diffuse scattering parallel to the ternary axis in the reciprocal space.

cubic pyrochlore structure contains the same proportion of A and B cations.

According to previous results (3–7), the 3 × 5 and 3 × 7 structures can be described, respectively, by the sequences …/$\mathcal{A}\alpha\mathcal{B}\beta\mathcal{C}/\mathcal{B}\beta\mathcal{C}\gamma\mathcal{A}/\mathcal{C}\gamma\mathcal{A}\alpha\mathcal{B}/$… and …/$\mathcal{A}\alpha\mathcal{B}\beta\mathcal{C}\gamma\mathcal{A}/\mathcal{C}\gamma\mathcal{A}\alpha\mathcal{B}\beta\mathcal{C}/\mathcal{B}\beta\mathcal{C}\gamma\mathcal{A}\alpha\mathcal{B}/$… shown in Figs. 7b and 7c. The stacking fault consists of the absence of one layer rich in B cations and consequently of the juxtaposition of two layers rich in A cations. Nevertheless, with respect to the relative positions of these layers around the stacking fault, it is more convenient to consider the fault as the absence of two layers rich in B cations and one layer rich in A cations. Then, it is straightforward to see that the higher the stacking fault density, the higher the [Pb]/[Ta] ratio. Hence, the 3 × 5 and 3 × 7 faulted structures lead, respectively, to the composition formulas $Pb_{2.44}Ta_2O_{7.44}$ and $Pb_{2.31}Ta_2O_{7.31}$. The 7 + 5 structure, which has never been reported in the literature, can be simply considered as the combination of two blocks constituting the two previous structures as …/$\mathcal{A}\alpha\mathcal{B}\beta\mathcal{C}/\mathcal{B}\beta\mathcal{C}\gamma\mathcal{A}\alpha\mathcal{B}/$… (Fig. 7d). In that case, the deduced composition is equal to $Pb_{2.36}Ta_2O_{7.36}$.

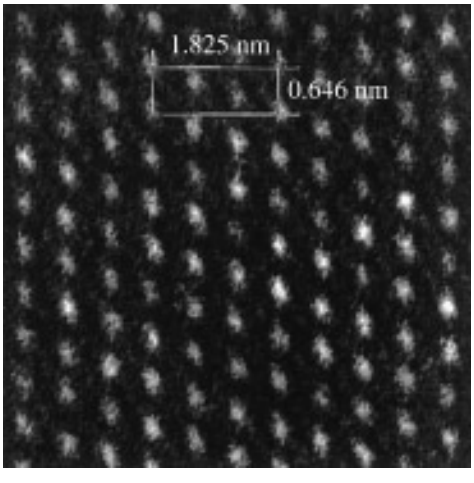

FIG. 5. Bright field image of the cubic pyrochlore phase (enlargement of Fig. 4). On the basis of a $d_{100_{hex}}$ equal to 0.646 nm, the c parameter is deduced to be equal to 1.825 nm.

In a general way, a block built with p layers constitutes an elementary cell when $p = 3n$ (p and n are integers). If p differs from $3n$, it is necessary to consider three blocks in order to obtain a periodic cell. This rule can be generalized to more complicated configurations, as superblocks, which are constituted themselves of N blocks with p_i layers. If $p_1 + \cdots + p_N = 3n$, the superblock is a cell (it is the case for the 7 + 5 phase) otherwise 3 superblocks are necessary in order to have a periodic cell. The problem of the cohesion between stacked blocks has been discussed by several authors on the basis of vibrational spectroscopy studies (17). By comparison with results related to different

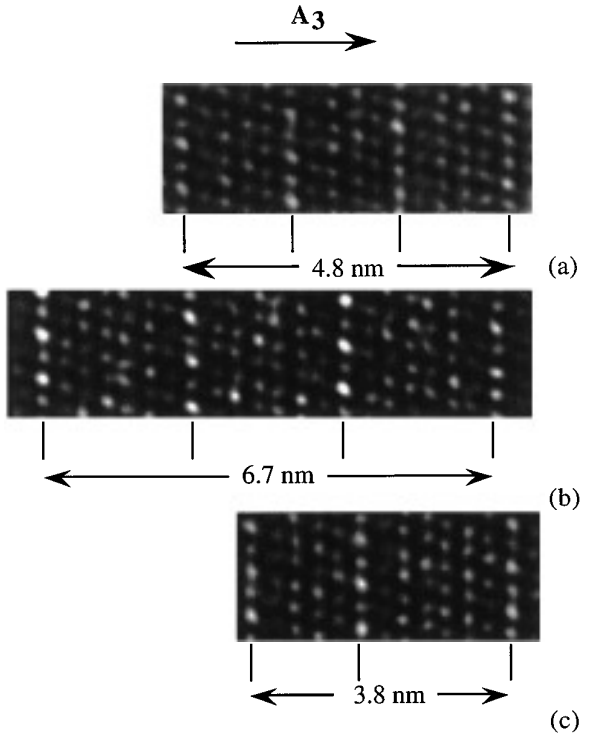

FIG. 6. HREM micrographs related to the different observed phases in PTO crystals. For each phase, the c parameter is deduced from the repetition of white dots along the ternary axis. It can then be deduced that the different structures consist in stacking of 3×5 (a), 3×7 (b), and $7 + 5$ layers (c).

lead oxides, e.g., PbO-α, PbO-β, and Pb_3O_4 (18, 19), it has been suggested that the cohesion blocks could be achieved by Pb–Pb quadrupolar interactions.

In order to confirm this structural model, HREM image simulations have been performed using a multislice algorithm in the EMS program (20). Since the contrast of the stacking faults is the same for the different faulted structures and does not seem to depend on the number of layers between successive faults, HREM simulations of the 7 + 5 structure has been achieved due to its relatively small c parameter.

The crystallographic structure model of the 7 + 5 structure used in the HREM simulation is constructed from the stacking sequence described above. The two blocks $/\mathcal{A}\alpha\mathcal{B}\beta\mathcal{C}/$ and $/\mathcal{B}\beta\mathcal{C}\gamma\mathcal{A}\alpha\mathcal{B}/$ derive directly from the ideal cubic pyrochlore structure.

In this model, all crystallographic sites are considered to be fully occupied. Nevertheless, in order to obtain electric neutrality, some oxygen vacancies are necessary. Focusing our attention on oxygen atoms, it can be seen that there are two types of oxygen sites: those belonging to the octahedral network TaO_6 (that we call O-type) and those lying in the tunnel formed by the octahedral network (O′-type). A preliminary hypothesis was to consider that, within blocks, the octahedral network is complete, e.g., that all O-type sites are occupied. This hypothesis is in agreement with structural analyses reported by Saine and Bernotat-Wulf related to lead niobates (3–7). Concerning the O′-type sites, several hypotheses can be considered with regard to their occupancy. HREM simulations have been performed using several different O′-type site occupancies with respect to the electrical neutrality and the comparison between the different hypotheses indicates that no difference could be seen over a wide range of defocii (Δf) and thickness (Δz) (Δf in the [0–200 nm] range and Δz in the [0.75–30 nm] range). It seems that the problem of the O′-site oxygen may not be solved easily with the TEM that we have used.

Comparison between experimental and simulated HREM images is shown in Fig. 8. In the considered model, O′-type sites lying within the blocks are supposed to be fully occupied and the vacancies are localized nearby the stacking faults. Due to symmetry considerations, an average site occupancy has been attributed to the oxygen sites lying nearby the stacking faults. Despite the noise observed

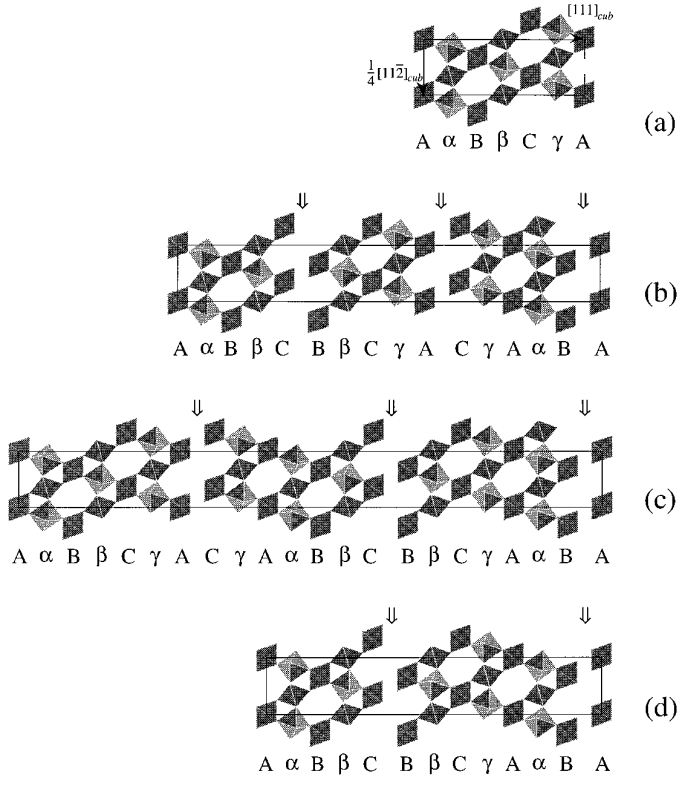

FIG. 7. Structural models related to the different observed structures. Only the octahedral layer is represented along equivalent directions (e.g., $[100]_{hex}$) and stacking sequences are reported below each structure. (a) Ideal cubic pyrochlore structure. Corresponding cubic directions are indicated. (b), (c), and (d): Structural models of the different faulted structures. Stacking faults are indicated by arrows.

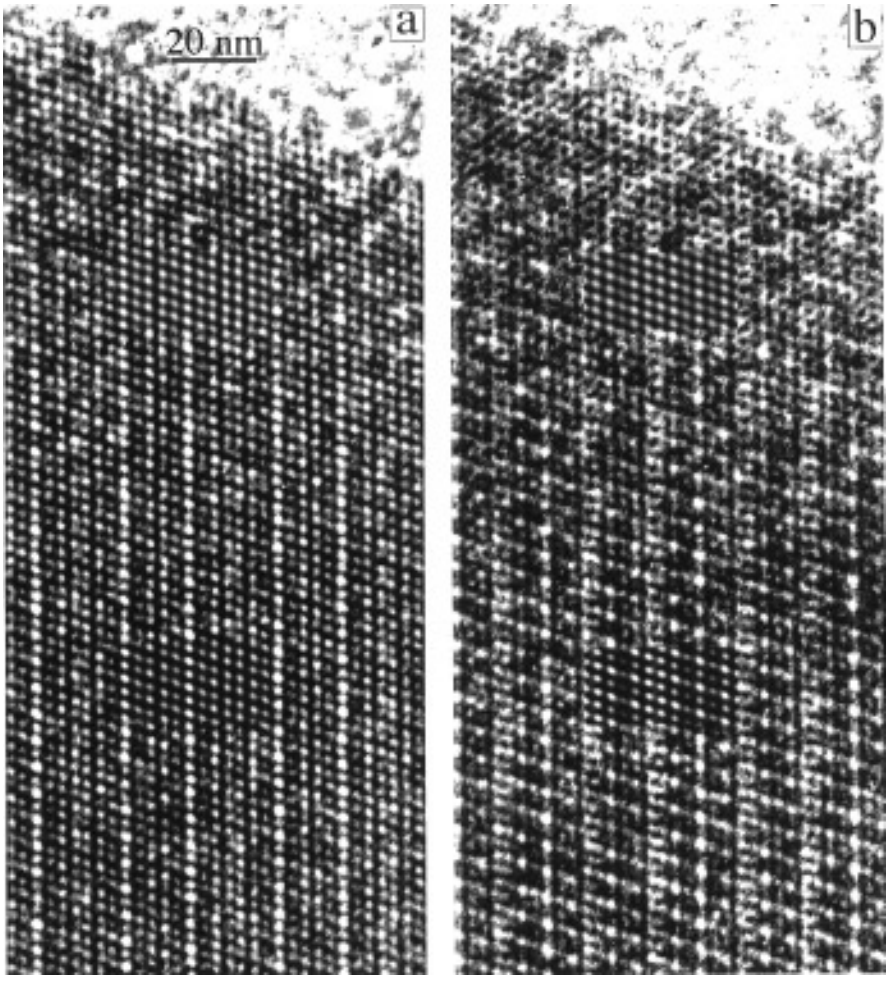

FIG. 8. Comparison between experimental and simulated HREM for the 7 + 5 structure. The thickness of the sample increases from top (edge of the sample) to bottom of the images. Defocalizations are, respectively, equal to $\Delta f = -160$ nm (a) and $\Delta f = -195$ nm (b). Inserted HREM simulations correspond to thickness parameters, respectively, equal to 4.5 and 12 nm.

on the image at the edge of the PTO particle and probably due to the specimen contamination and the presence of the carbon film, a reasonable match is observed between simulated and experimental HREM.

DISCUSSION

From the SADP results, only 4 different phases have been observed. Nevertheless, two experimental points have to be noticed:

(i) The TEM technique in general and the SADP technique in particular provide statistical results; e.g., it is impossible to certify that all the existing phases have been observed. The existence of other phases cannot be excluded especially since for the same composition range in the analogous $PbO–Nb_2O_5$ system, 1×9 and 3×11 phases have been observed (6, 15).

(ii) The number of observed defined phases depends also on the observation scale. By observed single phases, we mean phases in which the ordering of stacking faults is sufficiently developed to give rise to a well-defined SADP with sharp Bragg peaks for a given selected-area aperture diameter. Obviously, this depends of the selected-area aperture diameter and in our case, due to the selected-area aperture which was used, phases which are considered as defined single phases have a minimum size equal to 0.5 μm.

The most important point concerns the thermodynamic stability of the observed phases and consequently the existence of these phases in the $PbO–Ta_2O_5$ phase diagram. From an experimental point of view, the observation of such ordered phases as the 3×5, 3×7, and 7 + 5 phases leads us to assume that they are equilibrium phases. Indeed, the existence of the 7 + 5 phase, e.g., the regular alternation of two types of blocks, proves that the growth is controlled by the stoichiometry and, as a result, that

these phases are equilibrium phases with defined stoichiometry and crystallographic structure. Then, the existence of a solid solution in the $Pb_{2.31}Ta_2O_{7.31}$–$Pb_{2.44}Ta_2O_{7.44}$ composition range has to be excluded. The apparent nonstoichiometric behavior is due to the juxtaposition of intermediate compounds with closely spaced but clearly defined compositions. Moreover, the rhombohedral phase $Pb_2Ta_2O_7$ has not been observed and, as suggested by Scott, it seems that the existence of this phase has to be rejected.

CONCLUSION

The PbO–Ta_2O_5 phase diagram has been reinvestigated in the $Pb_{1.5}Ta_2O_{6.5}$–$Pb_{2.44}Ta2O_{7.44}$ composition range using TEM techniques. The apparent solid solution is due to the intergrowth of different structures derived from the host pyrochlore structure. In this composition range, the PbO–Ta_2O_5 system is quite similar to the PbO–Nb_2O_5 system. Moreover, structural models of the stacking faults observed in these structures and previously proposed for lead niobates have been confirmed from HREM observations and image simulations.

ACKNOWLEDGMENTS

The authors are grateful to A. Charaŕ, C. Alfonso, S. Giorgio, and A. Baronnet for fruitful discussions.

REFERENCES

1. J. S. Anderson, *in* "The Chemistry of Extended Defects in Non-Metallic Solids" (L. Eyring and M. O'Keefe, Eds.), p. 1. North-Holland, Amsterdam, 1970.
2. J. S. Anderson, *J. Phys. C7* **38,** 17 (1977).
3. M. C. Saine, R. Chevalier, and H. Brusset, *C.R. Acad. Sci. Paris Série C* **284,** 331 (1977).
4. M. C. Saine, G. Schiffmacher, M. Gasperin, and H. Brusset, *Rev. Chim. Minér.* **16,** 597 (1979).
5. M. C. Saine, *Thèse de Doctorat d'état ès Sciences Physiques, University Pierre et Marie Curie, Paris VI,* 1981.
6. H. Bernotat-Wulf and W. Hoffmann, *Z. Kristallogr.* **158,** 101 (1982).
7. H. Bernotat-Wulf and W. Hoffmann, *Naturwissenschaften* **67,** 141 (1980).
8. H. G. Scott, *J. Solid State Chem.* **43,** 131 (1982).
9. F. Jona, G. Shirane, and R. Pepinski, *Phys. Rev.* **98,** 903 (1955).
10. E. C. Subbarao, *J. Am. Ceram. Soc.* **44,** 92 (1961).
11. S. Kemmler-Sack and W. Rudorff, *Z. Anorg. Allg. Chem.* **344,** 23 (1966).
12. E. Aleshin and R. Roy, *J. Am. Ceram. Soc.* **45,** 18 (1962).
13. F. Thuriès, *Thesis, University of Aix-Marseille III,* 1995.
14. R. S. Roth, *J. Res. Nat. Bur. Stand.* **62,** 27 (1959).
15. M. C. Saine, M. Gasperin, and H. Brusset, *Rev. Chim. Minér.* **18,** 587 (1981).
16. J. L. Rivolier, *Thesis, University Claude Bernard, Lyon I,* 1994.
17. M. T. Vandenborne, E. Husson, and M. Chubb, *Spectrochim. Acta A* **40,** 361 (1984).
18. J. P. Vigouroux, E. Husson, G. Calvarin, and N. Q. Dao, *Spectrochim. Acta A* **38,** 393 (1982).
19. J. Galy, G. Meunier, S. Andersson, and A. Åström, *J. Solid State Chem.* **13,** 142 (1975).
20. P. A. Stadelman, *Ultramicroscopy* **21,** 131 (1987).